High-throughput identification of the spatial origins of *Drosophila* optic lobe neurons using single-cell mRNA-sequencing

Authors

Félix Simon[1], Isabel Holguera[1], Yen-Chung Chen[1], Jennifer Malin[1], Priscilla Valentino[2,3], Ted Erclik[2,3], and Claude Desplan[1]*.

[1]Department of Biology, New York University, New York, NY 10003, USA.
[2]Department of Biology, University of Toronto Mississauga, Mississauga, ON L5L 1C6, Canada.
[3]Department of Cell and Systems Biology, University of Toronto, Toronto, ON M5S 1A1, Canada.

*Correspondence: cd38@nyu.edu

Abstract

The medulla is the largest neuropil of the *Drosophila* optic lobe. It contains about 100 neuronal types that have been comprehensively characterized morphologically and molecularly. These neuronal types are specified from a larval neuroepithelium called the Outer Proliferation Center (OPC) via the integration of temporal, spatial, and Notch-driven mechanisms. Although we recently characterized the temporal windows of origin of all medulla neurons, as well as their Notch status, their spatial origins remained unknown. Here, we isolated cells from different OPC spatial domains and performed single-cell mRNA-sequencing to identify the neuronal types produced in these domains. This allowed us to characterize in a high-throughput manner the spatial origins of all medulla neurons and to identify two new spatial subdivisions of the OPC. Moreover, our work shows that the most abundant neuronal types are produced from epithelial domains of different sizes despite being present in a similar number of copies. Combined with our previously published scRNA-seq developmental atlas of the optic lobe, our work opens the door for further studies on how specification factor expression in progenitors impacts gene expression in developing and adult neurons.

Introduction

Animal brains rely on communication between specialized neuronal types that are each characterized by a specific set of features, both molecular (neurotransmitters, ion channels, etc.) and morphological (brain area targeted, synaptic partners, etc.).

The morphological diversity[1–4] of the *Drosophila* optic lobe neurons and their synaptic connectivity[5–8] have been comprehensively characterized. The *Drosophila* optic lobe is constituted of four neuropils (Fig.1A): the lamina, medulla, lobula and lobula plate. Each is subdivided into ~800 columns and, except for the lamina, in several layers orthogonal to the columns. Each column corresponds to the ~800 ommatidia of the retina and processes visual information from a single point in space. Optic lobe neuron arbors can be restricted to a unique column (narrow-field), in which case the neurons are often present in ~800 copies (synperiodic, *i.e.* one per column), or they can span multiple columns (wide-field), in which case the neurons are often present in smaller and variable numbers (infraperiodic), although any combination of these characteristics can be found across cell types.

Recently, we and others have characterized the molecular diversity of optic lobe neurons[9–13]. We performed single-cell mRNA sequencing (scRNA-seq) at 6 different stages of optic lobe development[9], and identified ~170 neuronal clusters. Almost ninety of these neuronal clusters and all glial clusters have since been matched to known cell types[9,14–18] (El-Danaf *et al.*, in preparation).

Understanding how the molecular and morphological features of each neuronal type are established is key to understanding brain development, and requires identifying how neuronal diversity is specified. The mechanisms specifying neuronal type identities have been characterized in great detail in the optic lobe[16,18–20]. Optic lobe neurons are produced from two crescent-shaped neuroepithelia at the third instar larval stage (L3, Fig.1B), the inner proliferation center and the outer proliferation center (OPC). The OPC can be further subdivided into the lateral OPC that produces the lamina, the tips of the OPC that express *wingless* (*wg*) and produce neurons in the medulla, lobula and lobula plate, and the main OPC (mOPC) that produces most medulla neurons (Fig.1B). The specification factors responsible for generating neuronal diversity have been characterized in detail[21] for the lateral OPC[22,23], the tips of the OPC[24] and the inner proliferation center[25–27]. In this work we focus on the mOPC, which generates the greatest neuronal diversity. At the beginning of the L3 stage, a neurogenic wave begins to convert mOPC neuroepithelial cells into neuroblasts that divide multiple times to self-renew and produce an intermediate progenitor called the ganglion mother cell, which in turn divides once more to generate two neurons. Neuronal identity is specified by the integration of three mechanisms[28–33]. First (Fig.1C), the mOPC neuroepithelium is subdivided into different spatial domains that express either *Visual system homeobox 1* (*Vsx1*), *Optix,* or *decapentaplegic* (*dpp*)[29]. Additionally, the dorsal part of the mOPC neuroepithelium express the *spalt* genes (*salm* and *salr*), while the ventral side expresses the *disco* genes (*disco* and *disco-r*) and, early in development, *hedgehog* (*hh*)[28,34]. We will hereafter refer to ventral and dorsal Vsx, Optix, and Dpp domains as v/dVsx, v/dOptix and v/dDpp, respectively. Second (Fig.1D), all mOPC neuroblasts sequentially express, as they age, a cascade of temporal transcription factors (tTFs), whose expression partially overlap[29–33]. Although only some tTFs maintain their expression in neurons, several downstream TFs termed "concentric genes" are expressed in neuronal types emerging from a given temporal window and are therefore expressed in a concentric fashion in the mOPC[32,35] (Fig.1D). Third (Fig.1E), the Notch pathway is active in one of the neurons produced by each ganglion mother cell ($Notch^{ON}$ neuron) but inactive in the other ($Notch^{OFF}$ neuron)[30]. We hereafter use "developmental origin" for any combination of spatial, temporal, and Notch origins. Based on a few examples, it was assumed that all $Notch^{ON}$ neurons were produced in all the mOPC spatial domains and were synperiodic, while $Notch^{OFF}$ neurons were produced in restricted spatial domains and were infraperiodic[19,29].

We recently described the temporal origin and the Notch status of all the mOPC clusters in our scRNA-seq atlas[32]. However, the lack of knowledge of their spatial origin has prevented us from exploring how the specification factors establish gene expression in developing neurons. In this study, we isolated all neurons produced from different mOPC spatial domains and performed scRNA-seq to identify them and thus characterize their spatial origin. Our results make the medulla the first complex brain structure for which the specification factors expressed in neural progenitors of each neuronal type are known. Moreover, these data allowed us to describe two new spatial domains, and to show that many synperiodic neurons are produced from restricted domains of the mOPC. Together, these resources will allow us to explore how the expression of specification factors in progenitors is relayed to downstream target genes during development to establish and maintain the specific features of optic lobe neurons.

Results

Profiling the neuronal types produced in each spatial domain

Traditionally, identifying the spatial origin of neuronal types has relied on the identification of combinations of TFs specific to a given neuronal type early in development and assessing their domain of expression in the larval mOPC, or by the overlap of spatial region-specific lineage tracing lines with reporter lines expressed in specific neurons in the adult[18,29,36]. However, such approaches are low-throughput, and it is not always possible to find such combinations. We therefore designed a high-throughput approach to identify the spatial origins of all mOPC neurons (Fig.2A). We drove the expression of nuclear GFP in cells produced from the various mOPC spatial domains using spatial region-specific *Gal4* drivers, isolated the labeled cells by Fluorescence-Activated Cell Sorting (FACS), performed scRNA-seq on the sorted cells, and annotated the cells from each population using a neural network classifier trained on our previously published optic lobe scRNA-seq atlas[9]. Whenever technically possible, we favored labelling and sequencing adult neurons by using memory cassettes (MC, Fig.2B, Fig.S1A, Methods) that label all progeny of cells that expressed a given *Gal4* driver earlier in development. Indeed, at early pupal stages some neurons are still immature and cannot be identified precisely by our classifier[9]. Moreover, when possible, we added a temperature-sensitive (TS) *Gal80*^{ts} to prevent later activation of the memory cassettes in developing neurons that do not originate from the domain of interest (Fig.2B, Fig.S1B, Methods).

We tested the specificity of the lines by checking their GFP expression pattern before neuronal somas are rearranged by migration[35] (Fig.2B, Fig.2C, Methods), *i.e.* either at the L3 larval stage or between 0 to 12.5% of pupal development (P0-P12.5). All lines labelled the expected mOPC populations and sometimes some cells outside the mOPC, which we accounted for in later analyses (see Methods). Some ectopic expression was observed in vOptix-MC (Fig.S1C, Fig.S1D), which we accounted for in later analyses, and in pxb-MC (Fig.S1E), which we eliminated by visually selecting optic lobes that did not exhibit ectopic expression before FACS and sequencing. We used *pxb-Gal4* rather than *Vsx-Gal4* because *Vsx* is also expressed in neurons from the v/dOptix domains (Fig.S1C, Fig.S1F).

The FACSed GFP-positive cells from each spatial domain were then subjected to scRNA-seq at the indicated stages (Fig.2B). We used our classifier[9] to annotate the transcriptome of each cell with a confidence score. For each dataset, we identified the "Classes" (defined hereafter as a group of cells with the same annotation) that were annotated with a lower confidence (Annex 1, Methods). We did not discard these cells but flagged them for later bioinformatic analyses, as low-confidence annotation scores are not always an anomaly and are, for instance, expected for subtypes with similar transcriptomes (Fig.S2A). We then normalized neuronal abundances to be able to compare them between different datasets (Fig.S2B). Although the spatial origin was very clear for most neuronal types (Fig.S2C, Annex 1), we sometimes found a low number of cells belonging to a neuronal type from a known spatial origin in datasets where they should be absent. This can be explained by experimental (*e.g.* imperfect sorting), bioinformatic (*e.g.* imperfect filtering), or biological (*e.g.* cell types with very similar transcriptomes, which are difficult to distinguish using the neural network) variations.

Identifying the spatial origin of optic lobe neurons

To facilitate the identification of false positives in each dataset and validate the scRNA-seq results, we used the known spatial origin of Dm8[36], Mi1[30,35], Pm1/2/3[29,29], T1[37] and TE[9] neurons, and experimentally validated the spatial origin of 33 additional clusters. To do so, we identified markers expressed early in these clusters (Fig.S3A) and assessed the location of their expression by immunostaining in the mOPC cortex at late L3 stage (before neurons migrate) (Fig.2D-F, Fig.S3B-J, Table S1). For instance, Mi9 expresses *svp* and *D*, and the co-expression of these markers was found in v/dOptix and in v/dDpp but not in v/dVsx at the L3 stage (Fig.2D), while Dm10 expresses *toy* and *tup,* which are only co-expressed in the ventral side of the mOPC (Fig.2E). This is consistent with the lack of Mi9 cells in our pxb dataset (Fig.S2C) and the lack of Dm10 cells in the dOptix dataset (Annex1), thus validating our scRNA-seq results.

We then computed the enrichment of each Class in each dataset (Fig.S2B) by dividing the normalized abundance of each Class by the normalized abundance in our previously published scRNA-seq atlas, which was used as a reference because it represents a largely unbiased sampling of optic lobe neurons from all mOPC domains. We binarized these enrichment values into "presence" or "absence" of a Class in a dataset by setting a threshold based on our experimental validations and the published origin of the cell types previously mentioned (Fig.S4 and S5, Annex 1, Methods). After binarization, only 2 neuronal types out of 40 for which we knew the spatial origin were found in an unexpected dataset (Fig.S4): Dm11 was found in the pxb dataset and Tm29 in the dpp dataset, in addition to being found in datasets containing cells from their expected origins (dOptix and d/vOptix domains, respectively, see TableS1). However, on UMAP visualization of these datasets, Dm11 and Tm29 are poorly separated from other Classes, which indicates that they are transcriptionally similar to other neuronal types and could have been misannotated by the neural network (Fig.S6, TableS1). Our results therefore highlight the high consistency between the spatial origins determined by scRNA-seq and the *in vivo* validations.

Moreover, Pm1 (cluster 163), and cluster 180 are both produced during the Hth temporal window and they express *TfAP-2* but not *Drgx* (Fig.S3A), and correspond to early-born neurons from the vOptix and v/dDpp domains (Fig.S3C). This is consistent (Table S1) with our scRNA-seq data that indicates production of cluster 163 in vOptix and cluster 180 in vDpp (and maybe dDpp), but it is not consistent with the previously described vDpp origin of Pm1[29]. This suggests that either we previously mis-annotated cluster 163 as Pm1[9], and instead cluster 180 corresponds to Pm1, or that the neuronal type we previously identified in the vDpp domain[29] was not Pm1 but instead was the neuronal type corresponding to cluster 180.

Lastly, we generated a table assigning a spatial origin to all mOPC clusters by considering normalized abundances, proximity to enrichment binarization thresholds, UMAP representation, annotation confidence and experimental results from our validations and from previous publications (Methods). Our assignments are explained in Table S1, while Fig.2G represents a summarized view of this table.

Control of neuronal abundance in the optic lobe

We previously proposed a model in which Notch^{ON} neurons are produced from all spatial domains and are synperiodic, while Notch^{OFF} neurons are infraperiodic and produced in restricted spatial domains[29]. This model holds true in the first temporal window (Hth), and for Notch^{ON} neurons of the second temporal window (Hth/Opa): Tm1/2/4/6 are Notch^{ON}, synperiodic, and produced from all mOPC domains (Fig.2G). However, this model does not apply to Notch^{OFF} neurons of the Hth/Opa temporal window, or to later temporal windows (Fig.2G), as exemplified

by Mi9: this synperiodic neuron is Notch^{OFF} and it is not produced in the v/dVsx domain (Fig.2D). In fact, for temporal windows later than Hth/Opa, most Notch^{ON} neurons are infraperiodic and all are produced in restricted parts of the mOPC. Moreover, out of the 15 largest clusters in our scRNA-seq atlas (Fig.2G, clusters containing more than 1000 cells), 7 are Notch^{OFF}, and 11 are produced from restricted mOPC domains. All of these clusters correspond to synperiodic neurons, except for the infraperiodic Dm10 and 4 clusters for which we do not know the abundance of the corresponding neuronal types (TmY3, cluster 82, Tm25, and Mi15). Even if these 4 neuronal types were infraperiodic, which is unlikely given the large size of their corresponding clusters, this result also argues against a model in which all synperiodic neurons are Notch^{ON} and produced from all spatial domains. However, consistent with our previous model, most Notch^{OFF} neurons have a low abundance, since 16/19 of the rarest neuronal types (clusters containing less than 250 cells) for temporal windows later than Hth/Opa are Notch^{OFF} neurons generated from a restricted mOPC domain. Moreover, as we explored in Malin et al.[18], the abundance of rare Dm neuronal types is correlated with the size of their spatial domain of origin.

Discovery of additional spatial subdivisions

Our scRNA-seq data suggested the existence of two further spatial domain subdivisions, which we verified experimentally. First, according to our sequencing results, Tm9d was produced from dOptix and dDpp domains and Tm9v from the vVsx and vOptix domains (Table S1). Such asymmetry for two subtypes of the same neuron was unexpected, but we indeed verified that Tm9v but not Tm9d markers were present in a new domain at the ventral border between the Vsx and Optix domains (Fig.2F, Fig.2H, hereafter called "vVsx border"). Second, although Dm1 and Dm12 markers mapped on both sides of the border between the vOptix and vDpp domains (Fig.S3G), and both were found in the vOptix dataset, only Dm12 (but not Dm1) were also found in the dpp dataset (Annex1). Indeed, we experimentally validated[18] that there exists a new domain that produces Dm12 but not Dm1, where *Optix* and *dpp* overlap. This experimental validation of two new subdomains (Fig.2H) predicted from our scRNA-seq data further emphasizes the accuracy of our results. However, it also emphasizes that our determination of spatial origin of the optic lobe neurons could be achieved with even higher resolution by incorporating these domains. For instance, vOptix can in fact be subdivided into 4 subdomains: the anterior third producing pDm8[36], the middle third producing yDm8[36], and the posterior third that is split into an Optix+/Dpp- region producing Dm1 and an Optix+Dpp+ region producing Dm12. These domains are partly established by *dpp* signaling, as we showed in Malin et al.[18].

Discussion

A large excess of neuronal types can be encoded by the known specification factors

This work completes our comprehensive description of the spatial, temporal, and Notch origins of all neuronal types in the mOPC. Previously, it was thought that the existence of 10 temporal windows, 2 Notch statuses, and 6 spatial domains (v/dVsx, v/dOptix, v/dDpp) resulted in the encoding of 120 potential neuronal types in the mOPC[29,32] (10x2x6), a reasonable number compared to the ~100 neuronal types thought to exist in the medulla[9,12,13]. Moreover, we proposed that synperiodic neurons ignored spatial patterning and were produced in the whole mOPC due to their Notch^{ON} status[29]. However, as can be seen in Fig.2G, most neuronal types are produced across

only a subset of several spatial domains, regardless of their Notch status. Moreover, the distinction between two given spatial domains can affect the production of some neurons but not others. For instance, Mi9 is produced in the Optix but not the Vsx domain, whereas Tm5c is produced across both the Optix and the Vsx domains (Fig.2D, Fig.2G). Similarly, the distinction between ventral and dorsal mOPC does not affect the production of all neurons: Mi9 is produced from both ventral and dorsal mOPC, while Dm1/4/12 are only produced from the ventral mOPC (Fig.2D, Fig.2G, Fig.S3G). Therefore, spatial patterning factors have the potential to encode considerably more than six spatial origins, which is compounded by the discovery of additional subdivisions of the spatial domains in this work and others[18,36]. Moreover, our determination of the temporal origin of mOPC neurons was conservative due to the use of only a subset of marker genes, which were sometimes insufficient to separate broad temporal windows into smaller ones[32]. Lastly, Arain et al.[16] recently discovered a fourth axis of neuronal specification, in which progenitors from the same spatial domain and in the same temporal window, but produced at different time points during larval development, generate different Ap- (and therefore most likely Notch^{OFF}) neuronal progeny[16].

Together, these results suggest that the specification factors could encode hundreds of neuronal types in the mOPC. Because only ~100 mOPC neuronal clusters were obtained by scRNA-seq studies[9,12], this suggests that many potential neuronal types are never produced or are culled during optic lobe development. In this regard, it should be noted that although many potential spatial origins exist (since neuronal types can be produced across a combination of spatial domains), for a given temporal window and a given Notch status the spatial domains producing each neuronal type must be mutually exclusive. This likely explains a large part of why the total number of neuronal types that can be encoded is superior to the number of neuronal types really produced. It also highlights the need for further studies exploring how the spatial domains used to produce neurons change across temporal windows (*e.g.* for instance Optix and Vsx for Tm5c, but Optix and not Vsx for Mi9).

Regulation of neuronal abundance in the mOPC

We previously proposed that synperiodic neurons were Notch^{ON} and produced from the whole mOPC[29]. This work shows that, on the contrary, about half of the synperiodic neurons are Notch^{OFF}, and most of them are produced in restricted spatial domains that vary in size: whole OPC for T1[37], v/dOptix and v/dDpp for Mi9, anterior two thirds of vOptix for p/yDm8[36]. Because neither the Notch status nor the size of the spatial domains correlate perfectly with the abundance of synperiodic neurons, their abundance could also be controlled by the length of the temporal window during which they are produced. For instance, the production of ~800 Mi1 from the entire mOPC neuroepithelium, and of ~800 Dm8 from a much smaller domain, can be explained if the neuroblasts produce Dm8 for a longer time-period than they produce Mi1. Although we have indeed shown that Dm8 are produced during a longer temporal window than Mi1[18], this model remains to be tested in detail. Additionally, this model implies that for a fixed length of temporal window, the size of the epithelial domains producing each neuronal type should be correlated with the abundance of the neuronal types. We have shown that this is indeed the case for the infraperiodic Dm neurons[18].

Acknowledgments

We thank all members of the Desplan laboratory and especially Mehmet Neset Özel for helpful feedback while working on the manuscript, and Nikolaos Konstantinides for critical reading of the manuscript. We also thank Rana El-Danaf and Katarina Kapuralin for granting us early access to their *wg* scRNA-seq dataset. The laboratory was supported by a grant from the National Eye Institute R01EY13012. F.S. was supported by New York University (MacCracken Fellowship and Dean's Dissertation Ph.D. Fellowship). I.H. was supported by a Human Frontier Science Program Postdoctoral Fellowship LT000757/2017-L and by a senior postdoctoral fellowship from the Kimmel Center for Stem Cell Biology. Y.-C.C. was supported by New York University (MacCracken Fellowship), by a NYSTEM institutional training grant (Contract #C322560GG), and by a Scholarship to Study Abroad from the Ministry of Education, Taiwan. J.M was supported by a NIH fellowship (F32EY028012) and a grant from the National Eye Institute (K99EY032269). T.E was supported by an NSERC Discovery Grant (RGPIN2015-06457). P.V was supported the Vision Science Research Program (University of Toronto: Ophthalmology and Vision Sciences and UHN), the Ontario Graduate Scholarship, and the Queen Elizabeth II/Pfizer Graduate Scholarship in Science and Technology.

Author contributions:

F.S. and C.D. conceived the project and wrote the manuscript. F.S., Y.-C.C., J.M, P.V and T.E. built and tested the spatial origin lines. F.S. produced and analyzed the scRNA-seq data. I.H. described the spatial region of origin of many medulla neurons and performed the experimental validation of the spatial origins from scRNA-seq data.

Declaration of Interests:

The authors declare no competing interests.

Data availability

All raw and processed data are available in GEO (GSE254562).

Figures

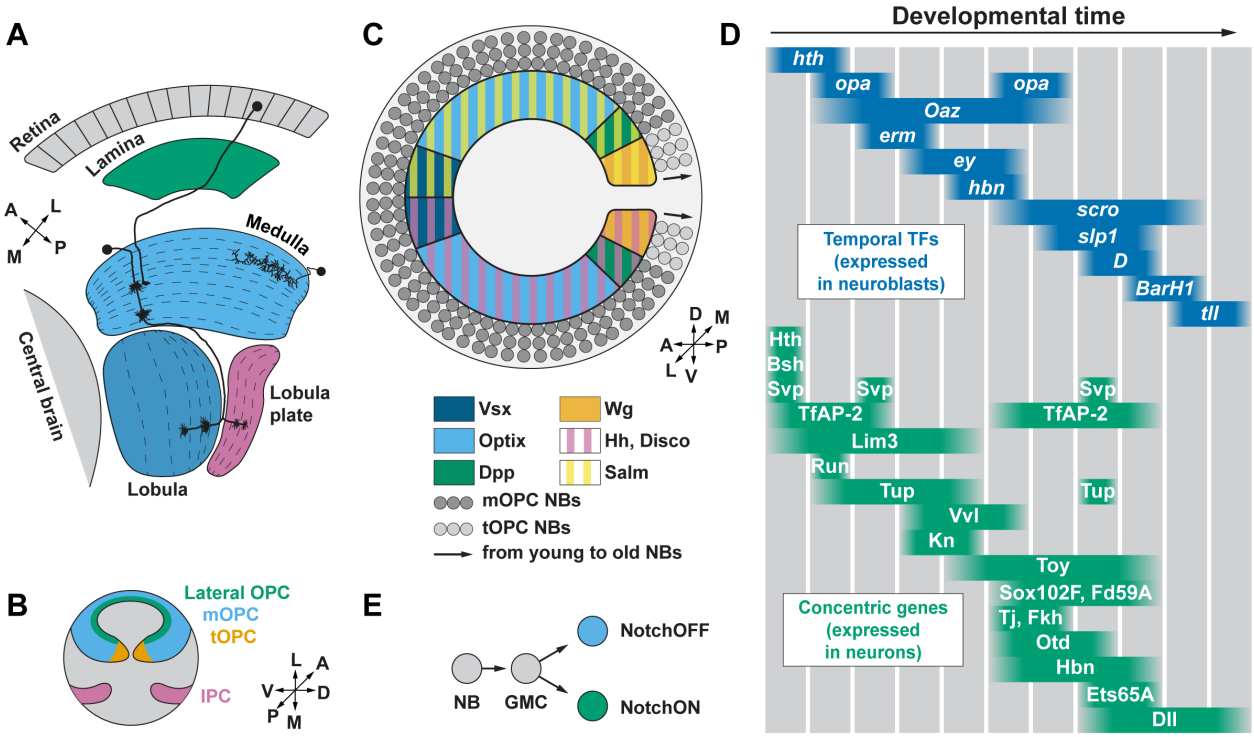

Figure 1: Specification of neuronal diversity in the *Drosophila* optic lobe.
A) Cross-section of the adult visual system, with neuropil labels located adjacent to each one. In black are represented two narrow-field neurons, including one photoreceptor (left), and one wide-field neuron (right). Dashed lines: boundaries between neuropil layers.
B) Schematic of the third instar larval optic lobe.
C) Spatial patterning of the mOPC, lateral view.
D) Temporal patterning of the mOPC. Each grey column represents a temporal window (Adapted from Konstantinides et al.[32]).
E) Diagram of Notch signaling in optic lobe neurons.
A: anterior, D: dorsal, GMC: ganglion mother cell, IPC: inner proliferation center, L: lateral, M: medial, NB: neuroblast, P: posterior, tOPC: tips of the OPC, V: ventral.

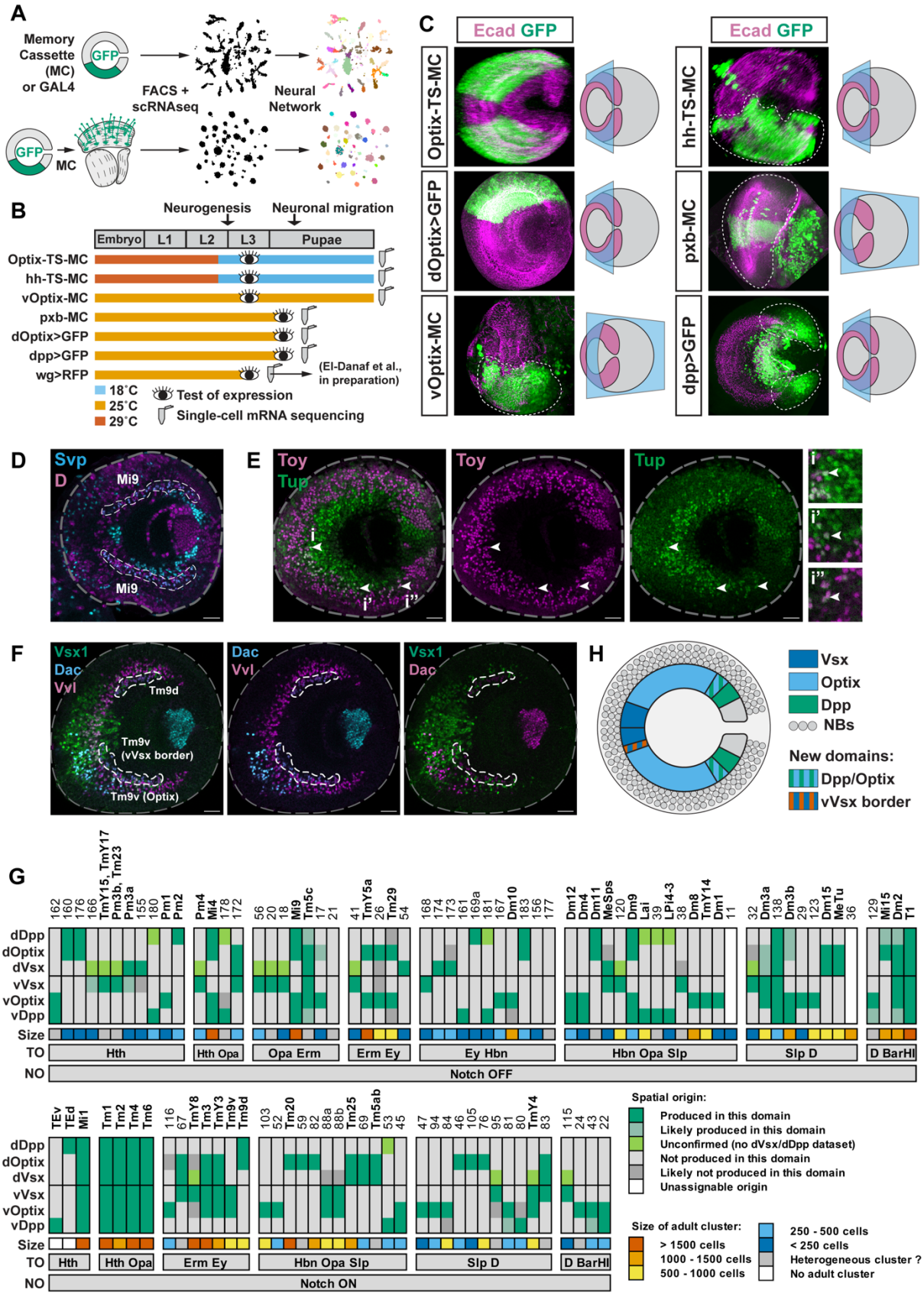
A
Memory Cassette (MC) or GAL4
GFP
FACS + scRNAseq
Neural Network
MC
B
Neurogenesis
Neuronal migration
Embryo
L1
L2
L3
Pupae
Optix-TS-MC
hh-TS-MC
vOptix-MC
pxb-MC
dOptix>GFP
dpp>GFP
wg>RFP
(El-Danaf et al., in preparation)
18˚C
25˚C
29˚C
Test of expression
Single-cell mRNA sequencing
C
Ecad GFP
Optix-TS-MC
dOptix>GFP
vOptix-MC
hh-TS-MC
pxb-MC
dpp>GFP
D
Svp
D
Mi9
E
Toy
Tup
i
i'
i''
F
Vsx1
Dac
Vvl
Tm9d
Tm9v (vVsx border)
Tm9v (Optix)
H
Vsx
Optix
Dpp
NBs
New domains:
Dpp/Optix
vVsx border
G
dDpp
dOptix
dVsx
vVsx
vOptix
vDpp
Size
TO
NO
Hth
Hth Opa
Opa Erm
Erm Ey
Ey Hbn
Hbn Opa Slp
Slp D
D BarHl
Notch OFF
Notch ON
Spatial origin:
Produced in this domain
Likely produced in this domain
Unconfirmed (no dVsx/dDpp dataset)
Not produced in this domain
Likely not produced in this domain
Unassignable origin
Size of adult cluster:
> 1500 cells
1000 - 1500 cells
500 - 1000 cells
250 - 500 cells
< 250 cells
Heterogeneous cluster ?
No adult cluster

Figure 2: Identification of the spatial origins of mOPC neurons using scRNA-seq.

A) Schematic of the approach used to identify the neurons produced in each mOPC domain.

B) Stages at which we tested the expression of, or sequenced, each of the lines used.

C) Maximum intensity z-projections showing the neurons labelled by each of the lines sequenced, following the protocol summarized on panel B. Labelled neurons outside of the dashed lines are not part of the mOPC. For orientation, see schematics and Fig.1C.

D-F) Expression of the indicated TFs in the OPC at the L3 stage, oriented as in Fig.1C. Grey dashed line: outline of optic lobe, white dashed line: regions of TF expression overlap in the temporal window corresponding to Mi9 or Tm9. Scale bars are 20 µm.

D) Mi9 neurons are Svp+ D+.

E) Toy+ Tup+ cells, which include Dm10 neurons, are indicated by arrows in the vVsx (i), vOptix (i'), and vDpp (i'') regions.

F) Tm9 neurons are the first row of Dac+ Vvl+ neurons.

G) Developmental origin (spatial, temporal, and Notch) and abundance of mOPC neuronal types. TO: temporal origin, NO: Notch origin, Size: number of cells comprised in the corresponding cluster in our adult scRNA-seq atlas[9].

H) Newly discovered spatial domains of the mOPC, lateral view.

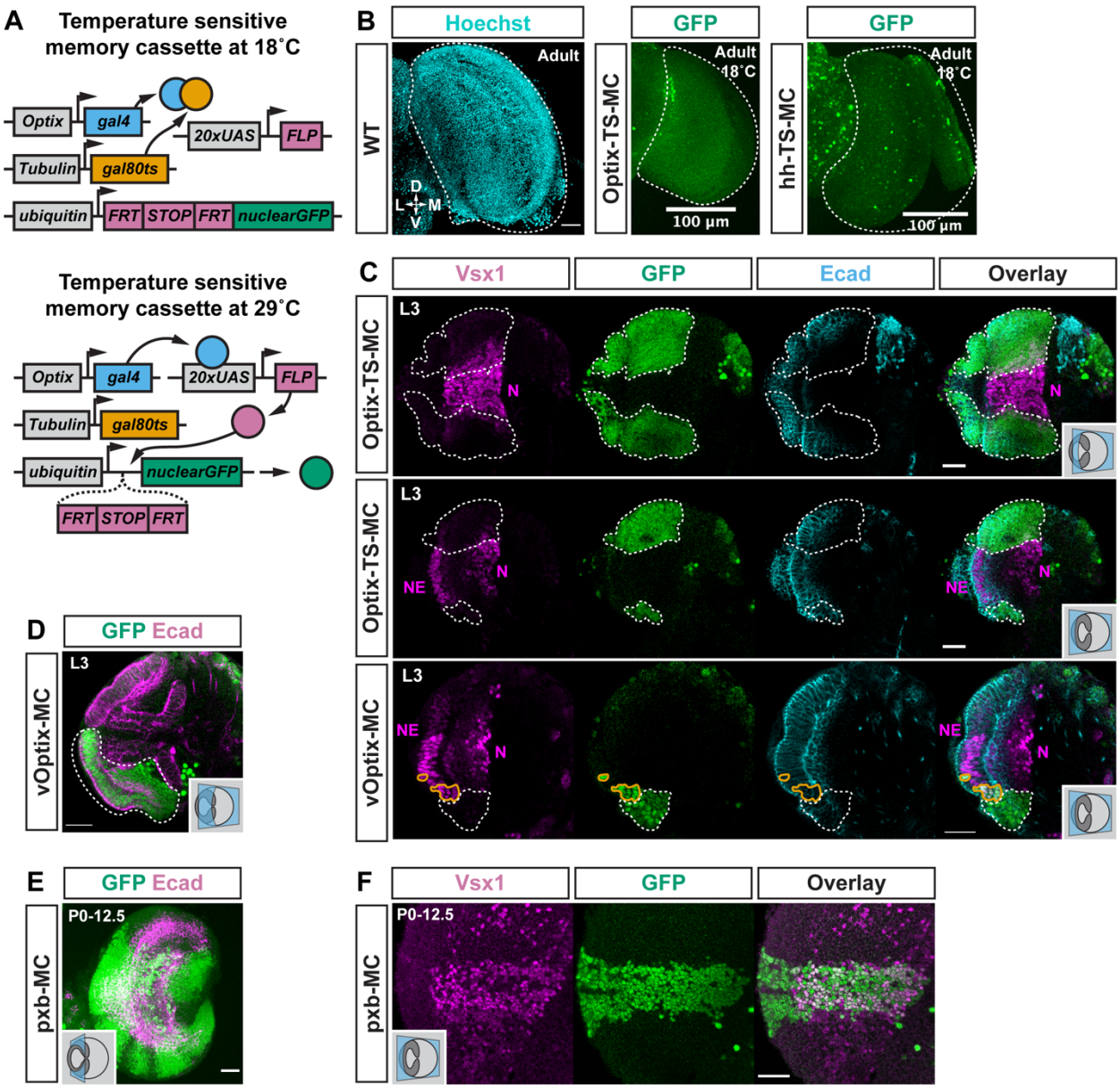
A
Temperature sensitive memory cassette at 18˚C
Optix
gal4
20xUAS
FLP
Tubulin
gal80ts
ubiquitin
FRT
STOP
FRT
nuclearGFP
Temperature sensitive memory cassette at 29˚C
Optix
gal4
20xUAS
FLP
Tubulin
gal80ts
ubiquitin
nuclearGFP
FRT
STOP
FRT
B
Hoechst
GFP
GFP
WT
Optix-TS-MC
hh-TS-MC
Adult
Adult 18˚C
Adult 18˚C
D
L
M
V
100 µm
100 µm
C
Vsx1
GFP
Ecad
Overlay
Optix-TS-MC
Optix-TS-MC
vOptix-MC
L3
N
NE
D
GFP Ecad
vOptix-MC
L3
E
GFP Ecad
pxb-MC
P0-12.5
F
Vsx1
GFP
Overlay
pxb-MC
P0-12.5

Supplementary figure 1: Characterization of the lines used to identify the spatial origin of mOPC neurons by scRNA-seq

A) Schematic describing how a temperature-sensitive memory cassette (MC) can be used to label all progeny of the cells expressing Gal4 (here driven by *Optix-Gal4*) when placed at the permissive temperature of 29˚C. Memory cassettes that are not temperature-sensitive lack the *tub-Gal80^{ts}* construct. In this case, it would label any cell that ever expressed *Optix-Gal4*, at any temperature, as well as its progeny.
B) Expression pattern of Optix-TS-MC and hh-TS-MC, in adult flies grown exclusively at 18˚C, and Hoechst labelling of an adult optic lobe. All images are maximum projections of 15 slices spanning the whole optic lobe, showing that the number of cells labelled in Optix-TS-MC and hh-TS-MC is negligible compared to the number of optic lobe nuclei, and that the Gal80^{ts} efficiently prevents activation of the MC. D: dorsal, L: lateral, M: medial, V: ventral. Labelled neurons outside of the dashed lines are not part of the optic lobe.
C) Top: Optix-TS-MC third instar larval expression pattern showing that some neurons from the Optix domain express Vsx1. Middle: additional view from the same brain showing that the Vsx domain neuroepithelial cells (high Vsx1+) are not labelled by the Optix-TS-MC line. Bottom: neuroepithelial cells from the vVsx border are labelled by the vOptix-MC line (circled in orange). N: neurons, NE: neuroepithelium. White dashed line: GFP expressed in the mOPC. For orientation, see schematics and Fig.1C.
D) In about 25% of the optic lobes, vOptix-MC labels the ventral tip of the OPC. Labelled neurons outside of the dashed lines are not part of the optic lobe. For orientation, see schematic and Fig.1C.
E) In some optic lobes, pxb-MC labels parts of the mOPC that were not produced in the Vsx domain (this shows an extreme example, at early pupal stage). We therefore checked the pattern of GFP expression of each optic lobe by epifluorescence microscopy before sequencing. However, due to the low resolution of this technique, it is conceivable that small amounts of false positive cells were not detected. For orientation, see schematic and Fig.1C.
F) pxb-MC expression pattern, showing that pxb-MC labels a band of Vsx1+ cells that corresponds to the Vsx domain at early pupal stage, and that pxb-MC does not label the Vsx1+ cells scattered in the Optix domain that can also be seen on Fig.S1C. For orientation, see schematic and Fig.1C.
(C-F) The immunostainings were done following the protocol summarized on Fig.2B. Unless indicated, all scale bars are 20 µm.

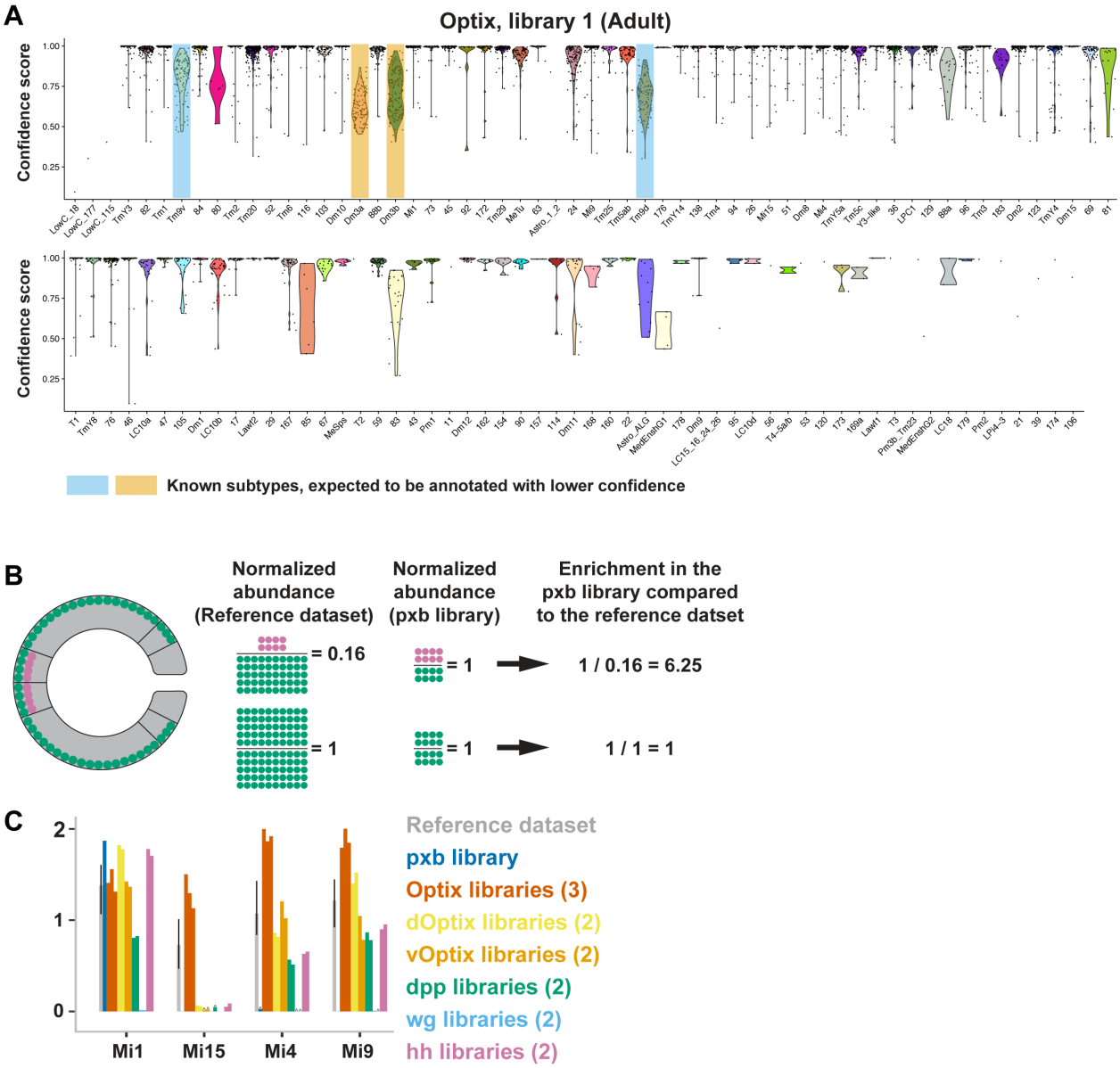

Supplementary figure 2: Annotation, normalization and filtering of the scRNA-seq libraries.
A) Confidence in the annotation of each cell type, grouped by Class, of one of the Optix libraries. This shows that although annotation confidence is high for most classes, it is (as expected) lower for classes corresponding to transcriptionally similar neurons (Dm3a/b, Tm9v/d). Classes with more than 80% of the cells with a score below 0.5 are prefixed with "LowC", *i.e.* "Low Confidence".
B) Schematic explaining the rationale of abundance normalization and enrichment scores. The normalized abundance of a neuron exclusively produced in the Pxb domain is higher in a dataset produced from the Pxb domain (whereas the number of cells, here 8 pink cells, is the same across both datasets). A reference dataset is a dataset containing neurons randomly sampled from all mOPC domains.
C) Normalized abundance of the indicated Medulla intrinsic (Mi) neurons in the different libraries.

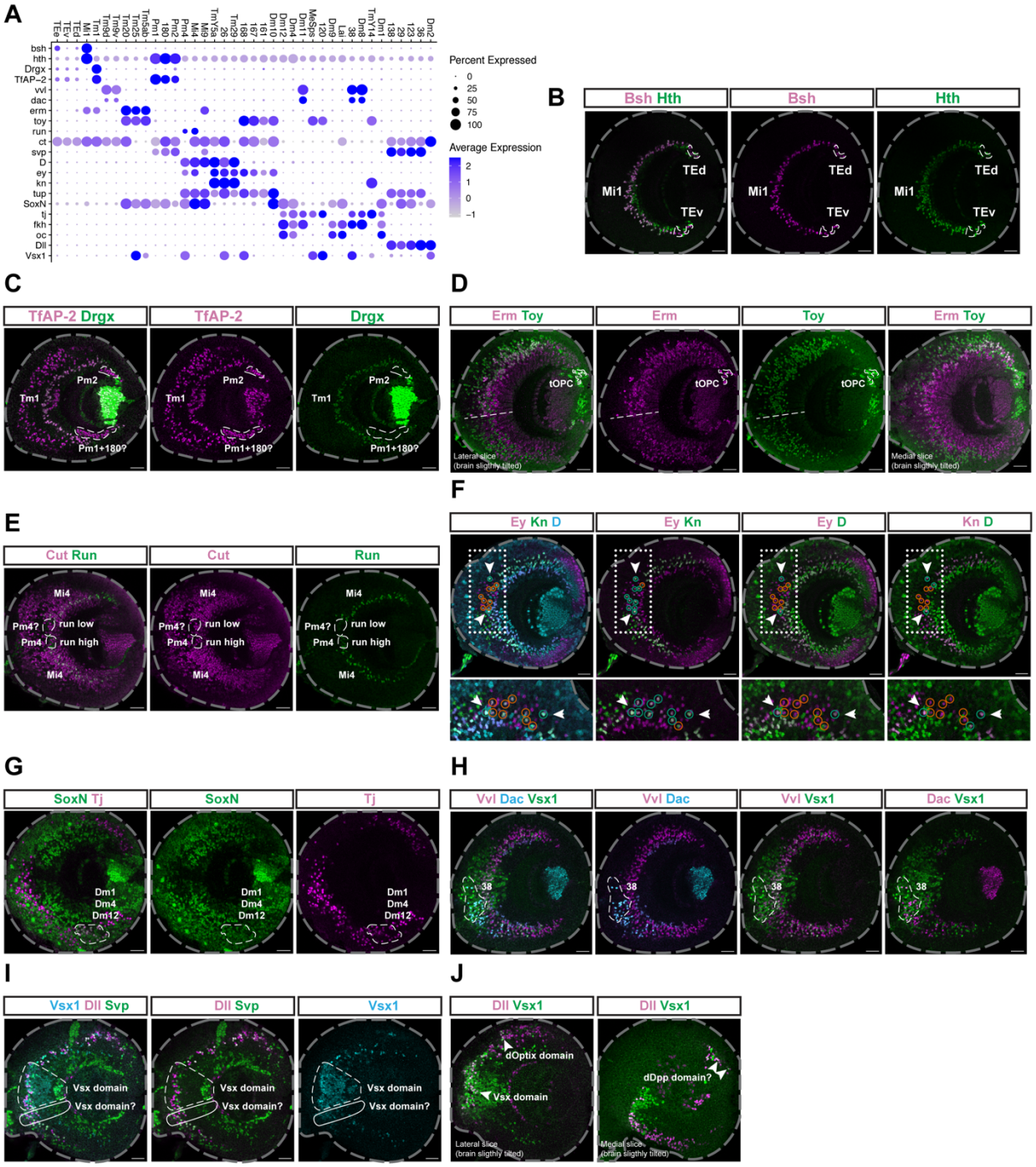
A
Percent Expressed
0
25
50
75
100
Average Expression
2
1
0
−1
B
Bsh Hth
Bsh
Hth
Mi1
TEd
TEv
C
TfAP-2 Drgx
TfAP-2
Drgx
Tm1
Pm2
Pm1+180?
D
Erm Toy
Erm
Toy
tOPC
Lateral slice
(brain slighly tilted)
Medial slice
(brain slighly tilted)
E
Cut Run
Cut
Run
Mi4
Pm4?
run low
Pm4
run high
F
Ey Kn D
Ey Kn
Ey D
Kn D
G
SoxN Tj
SoxN
Tj
Dm1
Dm4
Dm12
H
Vvl Dac Vsx1
Vvl Dac
Vvl Vsx1
Dac Vsx1
38
I
Vsx1 Dll Svp
Dll Svp
Vsx1
Vsx domain
Vsx domain?
J
Dll Vsx1
dOptix domain
Vsx domain
dDpp domain?

Supplementary figure 3: Experimental validation of the spatial origin of mOPC neurons

This figure shows the domain of expression of various TFs, used as markers to confirm the possible spatial origins from scRNA-seq data of various cell types. The marker used for each cell type, and how their expression was used to assess spatial origin, is detailed in Table S1.

A) Expression of the indicated TFs in the indicated neuronal clusters. For each neuronal cluster, their markers can be expressed in an mOPC domain larger than their spatial origin, because most of the markers are expressed in several neuronal clusters (some not shown in this panel).

B-J) Expression pattern of the indicated markers in the mOPC at the L3 stage. Grey dashed line: outline of the optic lobe, white dashed lines: localization of the labelled neurons (see Table S1), unless otherwise indicated. Scale bars are 20 µm.

D) Dashed line: estimation of the ventral border of the Vsx domain.

F) Cells in the Vsx domain are circled in green when they co-express the indicated markers, and circled in red when they do not. This shows that no cell expresses *ey*, *kn* and *D* in the Vsx domain, except maybe cells indicated by an arrowhead (these are uncertain because they are located at the limit of the Vsx domain). The white dotted lines correspond to the insets placed at the bottom, which are rotated 90 degrees clockwise to the original image.

I) The dashed white line indicates cells in the Vsx domain, while the solid white line indicates cells that might not be part of the Vsx domain.

J) The arrowhead indicates Dll+ Vsx1+ cells in the Vsx, dOptix and what is likely the dDpp domains.

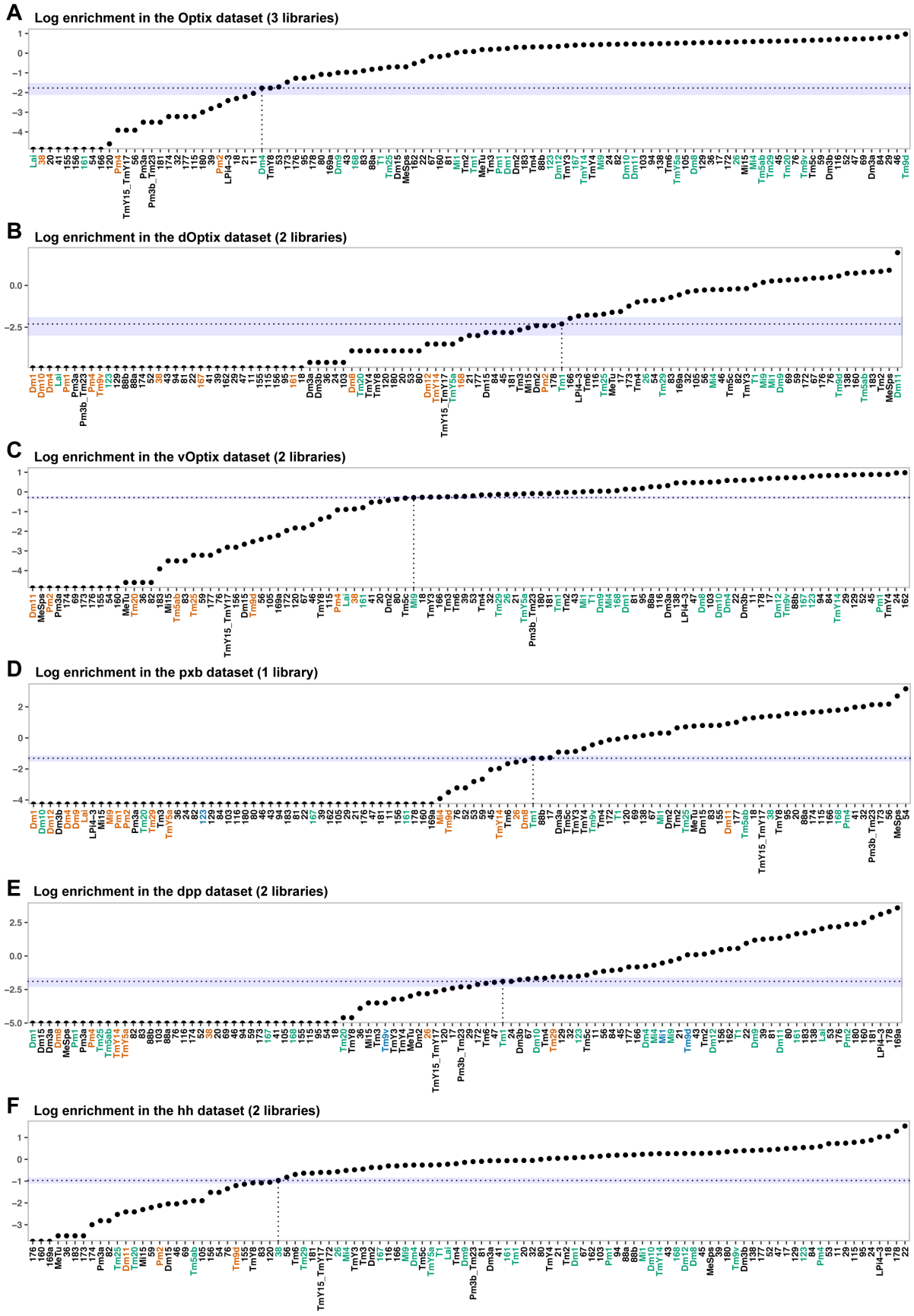
A
Log enrichment in the Optix dataset (3 libraries)
B
Log enrichment in the dOptix dataset (2 libraries)
C
Log enrichment in the vOptix dataset (2 libraries)
D
Log enrichment in the pxb dataset (1 library)
E
Log enrichment in the dpp dataset (2 libraries)
F
Log enrichment in the hh dataset (2 libraries)

Supplementary figure 4: Thresholds used to binarize the enrichment of mOPC neurons

A-F) Log-enrichment of the indicated Classes (x-axis) in each dataset. Enrichment was calculated by dividing the normalized abundances in the indicated datasets, by the normalized abundances in the Reference dataset. Vertical dotted lines: enrichment of the Class used as a threshold (represented by horizontal dotted lines) to binarize the enrichment values. Any class above this dotted line was considered as produced from the mOPC spatial domain corresponding to the dataset. Blue horizontal shaded regions: enrichment values close to the binarization threshold (Methods). The name of each neuronal Class is colored according to our validation experiments (Table S1). Red: neuronal types that should not be produced from the mOPC spatial domain corresponding to the indicated dataset, Green: neuronal types that could be produced from the mOPC spatial domain corresponding to the indicated dataset, Blue: neuronal types for which the presence in the corresponding mOPC domains was unclear.

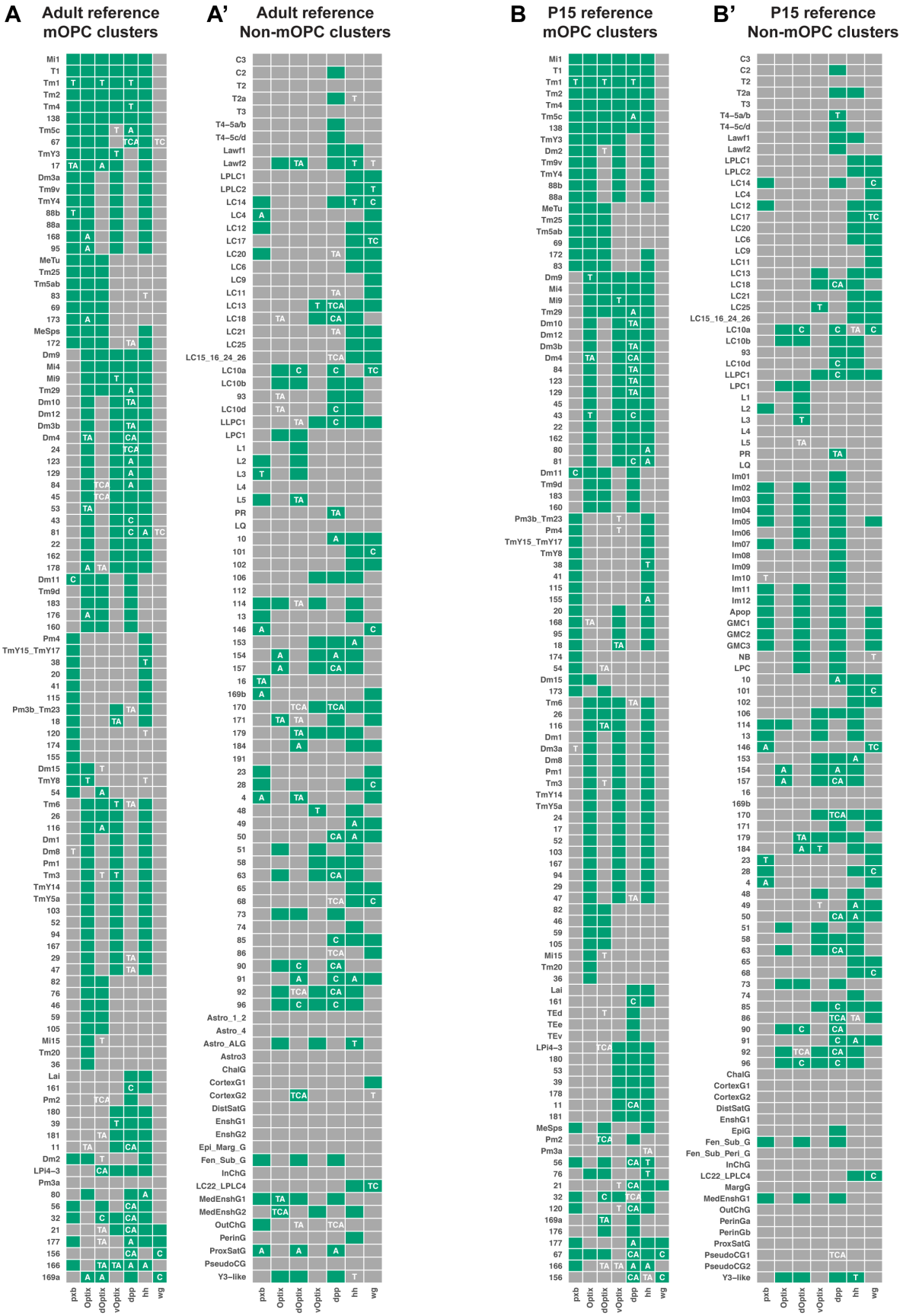
A
Adult reference
mOPC clusters
A'
Adult reference
Non-mOPC clusters
B
P15 reference
mOPC clusters
B'
P15 reference
Non-mOPC clusters
pxb
Optix
dOptix
vOptix
dpp
hh
wg

Supplementary figure 5: Binarized enrichment of the clusters in each dataset

A-B') Green squares: Classes (y-axis) considered as enriched in the corresponding dataset (x-axis) according to the binarization thresholds indicated in Fig.S4 (adult reference dataset) or Annex1 (P15 reference dataset). P15 was used as reference dataset in addition to the adult stage because TE neurons die before adulthood. Grey squares: Classes considered as depleted in the corresponding dataset. A = at least one of the libraries of the dataset had low abundance, *i.e.* contained fewer than 3 cells of this Class, C = at least 80% of the cells of the Class were annotated with a confidence score strictly below 0.5, T = the enrichment of the Class was close to the binarization threshold. Abbreviations used as cluster names are explained in Table S1 (the clusters ending with a capital G are glial clusters).

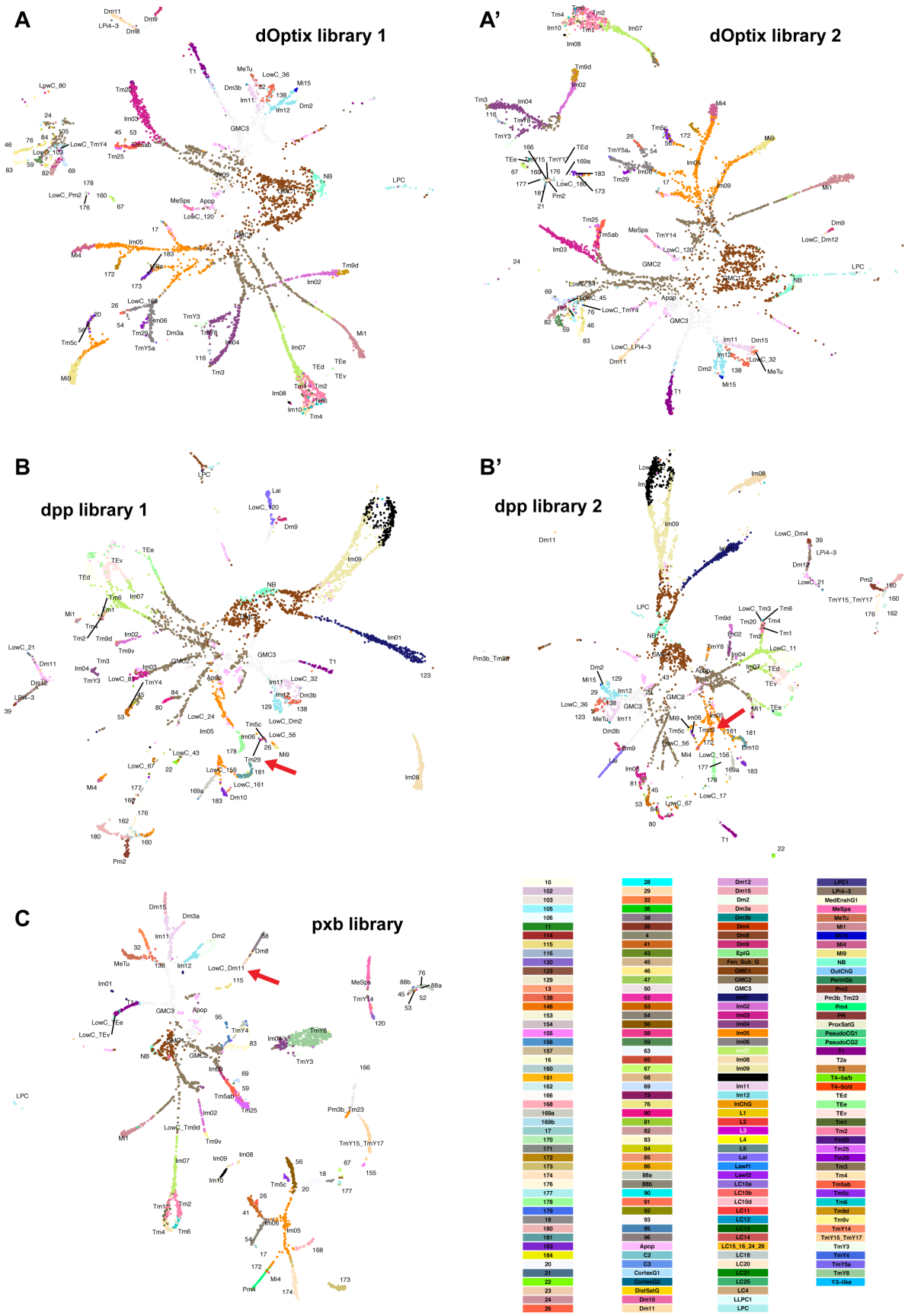
A
dOptix library 1
A'
dOptix library 2
B
dpp library 1
B'
dpp library 2
C
pxb library

Supplementary figure 6: UMAP visualizations of the libraries obtained at early pupal stages
A-C) UMAP plots obtained using 150 principal components. The cells are labeled and colored according to the key presented on the bottom right. Red arrows label Tm29 and Dm11 (see main text).

Methods

Obtaining the animals for scRNA-seq and testing GFP expression

The genotypes of the *Drosophila* lines used were:

- Optix-TS-MC line: *20xUAS-FlpG5::PEST; Optix-Gal4,tub-Gal80ts/CyO; ubi>STOP>Stinger/TM6*
- vOptix-MC line: *w*,disco-T2A-VP16AD; optix-T2A-Gal4DBD/+; UAS-Flp.D/UAS-Flp.Exel,UAS-RedStinger,Ubi>Stop>Stinger(G-Trace)*
- dOptix>Gal4: *w1118; salr-T2A-VP16AD,Optix-T2A-Gal4DBD/cyo*
- hh-TS-MC line: *20xUAS-FlpG5::PEST; ubi>STOP>Stinger/CyO; hh-Gal4,Gal80ts/TM6b,Tb*
- pxb-MC line: *20xUAS-FlpG5::PEST; ubi>STOP>Stinger/CyO-nlsGFP; pxb-T2A-Gal4/TM6b,Tb*
- dpp>GFP line: *w; (UAS-Stinger; dpp-Gal4)/[SM6a:TM6B, Tb, actGFP]*

For the Optix dataset, Canton S virgins crossed with Optix-TS-MC males were allowed to lay eggs for 2 hours at 18˚C. The eggs were then placed at 29˚C for 2 days and 9 hours (late L2 stage), then back at 18˚C for the reminder of their development. GFP expression was tested in L3 wandering larvae and sequencing was performed in adults (Fig.2B). We produced 3 libraries from the same cell suspension of optic lobes from 5 female flies that were a few hours old.

For the vOptix dataset, vOptix-MC flies were kept at 25˚C. GFP expression was tested in L3 wandering larvae and sequencing performed in adults (Fig.2B). We produced 2 libraries from the same cell suspension of the optic lobes of 15 female flies that were more than two-week-old.

For the dOptix dataset, *w; ; UAS-Stinger* virgins were crossed with dOptix>Gal4 males and kept at 25˚C. GFP expression was tested, and sequencing was performed, in P0-P12.5 pupae (Fig.2B). We produced 2 libraries from the same cell suspension of 24 optic lobes.

For the hh dataset, Canton S virgins crossed with hh-TS-MC males were allowed to lay eggs for 2 hours at 18˚C. The eggs were then placed at 29˚C for 2 days and 3 to 9 hours (mid to late L2 stage), then back at 18˚C for the reminder of their development. GFP expression was tested in L3 wandering larvae and sequencing was performed in adults (Fig.2B). We produced simultaneously 2 libraries from independently produced cell suspensions, each from the optic lobes of 7 two-week-old female flies.

For the pxb dataset, Canton S virgins were crossed with pxb-MC males and kept at 25˚C. GFP expression was tested, and sequencing was performed, in P0-P12.5 pupae (Fig.2B). We produced 1 library from 8 optic lobes.

For the dpp dataset, Canton S virgins were crossed with dpp>GFP males and kept at 25˚C. GFP expression was tested, and sequencing was performed, in P0-P12.5 pupae (Fig.2B). We produced simultaneously 2 libraries from independently produced cell suspensions, each from 6 optic lobes of young pupae.

All animals used for scRNA-seq were selected for the lack of balancer chromosomes. P0-P12.5 animals were obtained by selecting pupae in which the head had not yet detached from the pupal case[38].

For the wg dataset, the sequencing of the *wg-Gal4* line was performed in a different work (El-Danaf *et al.*, in preparation).

Sample preparation and single-cell mRNA-sequencing

We followed a similar cell dissociation protocol to generate all spatial domain datasets. Whole brains were extracted in ice-cold Schneider's media. The brains were then transferred into DPBS. We used an epifluorescence microscope to remove brains with ectopic mOPC GFP expression (we only found some for the pxb dataset, see main text), and placed the brains back in Schneider's media. The brains were then incubated at 25˚C in Schneider's media with 2 mg/mL Collagenase and 2 mg/mL Dispase, for 1 hr 30 min (adult brains) or for 30 min (pupal brains), then washed 3 times with ice-cold Schneider's media to stop the dissociation. Optic lobes were then separated from the central brain, transferred to ice-cold DPBS + 0.04% BSA, and washed twice with ice-cold DPBS + 0.04% BSA. For pupal brains, the separation between central brain and optic lobes can be seen as a difference in texture: the optic lobe forms a smoother and cohesive structure that can be removed using a fine tungsten needle. Optic lobes and 150 µL of DPBS + 0.04% BSA were then transferred to a low-bind Eppendorf, and dissociated by pipetting vigorously 50 times, resting the cells for 1 minute on ice, and pipetting 50 times more. The cell suspension was then checked under a dissecting microscope, and we pipetted up to 50 more times if the size of remaining clumps was too big. We did not try to dissociate small clumps since they are most likely neuropils, not soma, and indeed we empirically noticed a better quality of the data obtained after lowering pipetting repetitions. The suspension was then passed through a 20 µm mini-PluriStrainer, and the filter was washed with 400 µL of DPBS + 0.04% BSA which we also collected (pipetting from the opposite side may be necessary to collect the entire cell suspension).

Stinger (nuclear GFP)-positive cells were sorted by FACS, and we loaded the single-cell sequencing chip with 43.5 µL of the cell suspension provided by the FACS, undiluted, mixed with the master mix. Moreover, we used a tip coated with 70 µL of DPBS + 0.04% BSA and 0.02% Tween-20 to sample the cell suspension, and kept the same tip to load the chip, which we empirically noticed drastically reduces the loss of cells. All steps of single-cell sequencing were performed following the Chromium Next GEM Single Cell 3′ Reagent Kits v3.1 (Dual Index).

Supervised annotation of the scRNA-seq datasets:

The libraries were analyzed using Seurat 4.0.1. For each library, a Seurat Object was created with all genes expressed at least in 3 cells, and all cells expressing at least 200 genes. The objects were then filtered by keeping all cells below a certain percentage of mitochondrial genes, below a certain number of UMIs, and above a certain number of genes, chosen according to the distribution of these parameters (Annex 1). The thresholds chosen were identical for all libraries acquired at a given day with flies of a given genotype, but were different otherwise. For the Optix libraries the thresholds were 7/17000/800 (percent of mitochondrial genes, number of UMIs, number of genes), for the vOptix libraries 7/10000/500, for the dOptix libraries 5/20000/1000, for the hh libraries 10/20000/700, for the dpp libraries 5/20000/900, for the pxb library 5/30000/1300, for the wg libraries 10/25000/1200. After filtering, we obtained an Optix dataset of 19,036 cells (3 libraries), a hh dataset of 8,943 cells (2 libraries), a vOptix dataset of 10,494 cells (2 libraries), a dOptix dataset of 12,302 cells (2 libraries), a pxb dataset of 4,933 cells (1 library), a dpp dataset of 12,506 cells (2 libraries), and a wg dataset of 12,974 cells (2 libraries). For each library we then ran NormalizeData, FindVariableFeatures, and ScaleData with default parameters, as well as RunPCA, RunTSNE, and RunUMAP with default parameters and a dimensionality of 150. Dimensionality reductions were run purely for visualization purposes; they were not used to

perform any clustering. Instead, we used the normalized expression of marker genes and our neural network classifier[9] to assign each cell of each library from this study to its corresponding cluster in our previously published scRNA-seq atlas[9] (metadata fields "NN_Cluster_Number"), and to give this assignment a confidence score between 0 and 1 (metadata field "Confidence_NN_Cluster_Number"). For all figures, we replaced cluster numbers by cluster annotations (metadata fields "Annotation") using TableS2. Lastly, if at least 80% of the cells of a given Class were annotated with a confidence score strictly below 0.5, the Class was flagged as "low confidence" by assigning it the value "1" in the metadata field "cells_flagged", and its annotation was changed from "X" to ""LowC_X".

Binarization of the spatial origin of each mOPC cluster

We then normalized the abundance of each neuronal Class in each dataset. Indeed, a neuron produced exclusively in the Vsx domain is expected to be relatively more abundant in a library produced from sorted pxb cells compared to our published atlas, which contains neurons produced in all domains. However, a neuron produced in each domain equally should have a similar abundance in all datasets (Figure S2B). To allow comparisons of Class abundances between libraries, we used the abundances of neurons produced in the whole mOPC, since they represent a constant between mOPC domains. In each library, we therefore divided the abundance of each Class by the abundance of all the Classes corresponding to neuronal clusters produced in all the mOPC. We also normalized the abundance of each Class in our single cell atlas but averaged the normalized abundance across all libraries to simplify the comparisons. We performed a first round of normalization using Mi1, Tm1 and T1 (TableS1). We then used the results of this round of normalization to determine that T1, Mi1, Tm1, Tm2, Tm4, Tm5c, Tm6, and cluster 138 were produced in all mOPC domains and therefore used them for a second round of normalization. Because this second round of normalization did not show additional neurons produced in the whole mOPC, we did not perform further rounds of normalization. However, these clusters are not produced in the wg domain, so they could not be used to normalize wg libraries. We therefore only normalized this dataset by dividing the abundance of each Class by the abundance of its most abundant cluster.

However, normalized abundances are not enough to decide whether a neuronal type is produced in a given domain, because rare cell types would still represent only a small part of any dataset (for instance cluster 38 is produced in the vVsx region, which represents only half of the Vsx domain and thus the pxb dataset). We therefore computed an enrichment score for each Class in each spatial domain (Fig.S2B). To do so, we divided the average normalized abundance of a Class in all libraries of a spatial domain dataset by its average normalized abundance in our single cell atlas. Theoretically, any score above 1 should indicate an enrichment of the Class in a mOPC domain compared to the whole mOPC, and therefore indicate that this cluster is produced in this domain. However, for a given Class, the minimal and maximal normalized abundances across libraries of a same mOPC domain are usually variable (see Annex 1), probably due to technical reasons (dissociation, FACS…), and therefore enrichment scores could not be analyzed in such a straightforward manner.

Therefore, we then binarized these "enrichment scores" by choosing thresholds based on our experimental validations of spatial origin (Fig.S4). For the Optix dataset, we chose Dm4 as a threshold because this is the least abundant neuronal type that we ascertained to come from this domain. For the dOptix dataset, we chose Tm1 as a threshold instead of TmY5a or Tm20 (that we

know are produced in the dOptix domain), because some of these might have been annotated as immature neurons (with which they form a trajectory on UMAP visualization, Fig.S6). For the vOptix dataset, we chose Mi9 as a threshold instead of cluster 161, because cluster 161 is a very small cluster that is unlikely to be produced in all of the vVsx, vOptix and vDpp domains (which is where we found the expression of the markers for cluster 161, 167, 168, and Dm10, Table S1). For the pxb and dpp datasets, we chose Tm1 as a threshold because out of all the neuronal types we experimentally validated as coming from these domains, Tm1 was the least abundant in both the pxb and dpp datasets. For the hh dataset, we chose cluster 38 as a threshold because we know it is produced exclusively in the ventral OPC. We did not choose Tm5ab because 1) this cluster contains two cell types, and 2) their markers (shared with other clusters) are found in the d/vVsx, dOptix and dDpp: the ventral mOPC represent only a small part of their potential domain of production.

We performed all these analyses using both our scRNA-seq atlas at the P15 and adult stages as a reference, because some clusters (for instance the TE cells) are only found at one of the two stages. However, we favored results obtained with the adult dataset, because it contains more cells, and at this stage their identities are more defined (there are no more immature, unclassified, neurons). Moreover, we performed these analyses for both mOPC and non-mOPC clusters but displayed these clusters separately in our plots. The presence of non-mOPC neurons in our datasets can mean that 1) the neuron is produced outside the mOPC but still expressed our reporters, 2) the neuron is in fact produced in the mOPC and was mistakenly assigned as non-mOPC neurons[32].

Final determination of the developmental origin of mOPC clusters

We primarily used binarized enrichment to assign an origin to each Class. However, we deemed the binarized enrichment of a Class in a given dataset as less trustworthy if a class was flagged as being annotated with low confidence, and/or there were 3 cells or fewer of this class found in the dataset, and/or its enrichment value was +/- 0.05 compared to the binarization threshold (Fig.S5). In this case, we also considered additional parameters (see Table S1), for instance its localization on the UMAP (Fig. S6). For instance, if "ClassA" contains only a few cells annotated with low confidence, and its cells are mixed on the UMAP with cells from "ClassB" that are annotated with high confidence, it is likely that ClassA cells are in fact ClassB cells misannotated by the neural network. Our choices are explained in Table S1. Lastly, it should be noted that in the absence of dVsx and dDpp datasets, assignment to these regions could only be extrapolated. For instance, if a Class was found in the dpp and the hh datasets, it is clearly produced in vDpp, and maybe in dDpp. However, if the Class was also found in the vOptix and dOptix datasets, then the corresponding neuron is very likely to be also produced in the dDpp domain. Such determinations are also explained in TableS1.

Immunohistochemistry

Whole brains were dissected in Schneider's media and transferred to Schneider's media on ice for no more than 30 min. They were then fixed using 4% paraformaldehyde diluted in PBS 1X, for 20 min at room temperature. They were then rinsed 3 times in 0.5% Triton-X diluted in PBS 1X (PBTx), and then washed for 30 min in PBTx. Then, the brains were incubated at least 30 min in PBTx with 5% horse or goat serum (PBTx-block) at room temperature, and incubated at 4˚C for 1-2 overnights in primary antibodies diluted in PBTx-block. They were then rinsed 3 times in

PBTx, incubated two times for 30 min in PBTx, and incubated at 4˚C overnight in secondary antibodies diluted in PBTx-block. Lastly, they were rinsed 3 times in PBTx, incubated two times for 30 min in PBTx, and mounted in Slowfade before imaging with a Leica SP8 confocal microscope using a 63x glycerol objective. Images were processed in Fiji and Illustrator.

The following primary antibodies were used: mouse anti-Svp (1:20) (DSHB), mouse anti-tup (1:100) (DSHB), mouse anti-Dac 2-3 (1:40) (DSHB), mouse anti-Cut (1:10) (DSHB), rabbit anti-Dichaete (1:500) (modEncode), rabbit anti-toy (1:500)[9], rabbit anti-Bsh (1:1800)[9], rat anti-vvl (1:50)[32], guinea pig anti-Vsx1 (1:100)[15], guinea pig anti-Hth (1:500) (gift from Richard Mann), guinea pig anti-TfAP-2 (1:100)[32], rat anti-drgx (1:250)[15], rat anti-erm (1:100)[32], guinea pig anti-run (1:500)[32], rat anti-Ey (1:100), guinea pig anti-Kn (1:100)[32], rabbit anti-SoxN (1:250)[15], guinea pig anti-Tj (1:250) (gift from Dorothea Godt[39]), rabbit anti-Dll (1:100)[32].

The following secondary antibodies, all from donkey, were used: anti-rat DyLight 405 (1:100), anti-rabbit DyLight 405 (1:100), anti-guinea pig DyLight 405 (1:100), anti-mouse Alexa Fluor 488 (1:400), anti-mouse Alexa Fluor 555 (1:400), anti-guinea pig Cy3 (1:400), anti-rabbit Alexa Fluor 555 (1:400), anti-rat Alexa Fluor 647 (1:200), anti-rabbit Alexa Fluor 647 (1:200), and anti-guinea pig Alexa Fluor 647 (1:200).

References

1. Fischbach, K.-F. & Dittrich, A. P. M. The optic lobe of Drosophila melanogaster. I. A Golgi analysis of wild-type structure. *Cell Tissue Res.* **258**, 441–475 (1989).
2. Wu, M. *et al.* Visual projection neurons in the Drosophila lobula link feature detection to distinct behavioral programs. *eLife* **5**, e21022 (2016).
3. Nern, A., Pfeiffer, B. D. & Rubin, G. M. Optimized tools for multicolor stochastic labeling reveal diverse stereotyped cell arrangements in the fly visual system. *Proc. Natl. Acad. Sci.* **112**, E2967–E2976 (2015).
4. Otsuna, H. & Ito, K. Systematic analysis of the visual projection neurons of Drosophila melanogaster. I. Lobula-specific pathways. *J. Comp. Neurol.* **497**, 928–958 (2006).
5. Rivera-Alba, M. *et al.* Wiring economy and volume exclusion determine neuronal placement in the Drosophila brain. *Curr. Biol. CB* **21**, 2000–2005 (2011).
6. Takemura, S. *et al.* Synaptic circuits and their variations within different columns in the visual system of Drosophila. *Proc. Natl. Acad. Sci. U. S. A.* **112**, 13711–13716 (2015).
7. Takemura, S. *et al.* A visual motion detection circuit suggested by Drosophila connectomics. *Nature* **500**, 175–181 (2013).
8. Dorkenwald, S. *et al.* Neuronal wiring diagram of an adult brain. 2023.06.27.546656 Preprint at https://doi.org/10.1101/2023.06.27.546656 (2023).
9. Özel, M. N. *et al.* Neuronal diversity and convergence in a visual system developmental atlas. *Nature* **589**, 88–95 (2021).
10. Konstantinides, N. *et al.* Phenotypic Convergence: Distinct Transcription Factors Regulate Common Terminal Features. *Cell* **0**, (2018).
11. Davis, F. P. *et al.* A genetic, genomic, and computational resource for exploring neural circuit function. *eLife* **9**, e50901 (2020).

12. Kurmangaliyev, Y. Z., Yoo, J., Valdes-Aleman, J., Sanfilippo, P. & Zipursky, S. L. Transcriptional Programs of Circuit Assembly in the Drosophila Visual System. *Neuron* S0896627320307741 (2020) doi:10.1016/j.neuron.2020.10.006.
13. Simon, F. & Konstantinides, N. Single-cell transcriptomics in the Drosophila visual system: Advances and perspectives on cell identity regulation, connectivity, and neuronal diversity evolution. *Dev. Biol.* **479**, 107–122 (2021).
14. Ferreira, A. A. G. & Desplan, C. An Atlas of the Developing Drosophila Visual System Glia and Subcellular mRNA Localization of Transcripts in Single Cells. 2023.08.06.552169 Preprint at https://doi.org/10.1101/2023.08.06.552169 (2023).
15. Özel, M. N. *et al.* Coordinated control of neuronal differentiation and wiring by sustained transcription factors. *Science* **378**, eadd1884 (2022).
16. Arain, U., Islam, I. M., Valentino, P. & Erclik, T. Concurrent temporal patterning of neural stem cells in the fly visual system. 2022.10.13.512100 Preprint at https://doi.org/10.1101/2022.10.13.512100 (2022).
17. Chen, Y.-C. D. *et al.* Using single-cell RNA sequencing to generate predictive cell-type-specific split-GAL4 reagents throughout development. *Proc. Natl. Acad. Sci.* **120**, e2307451120 (2023).
18. Malin, J. A., Chen, Y.-C., Simon, F., Keefer, E. & Desplan, C. Spatial patterning regulates neuron numbers in the Drosophila visual system. 2023.08.28.555170 Preprint at https://doi.org/10.1101/2023.08.28.555170 (2023).
19. Sen, S. Q. Generating neural diversity through spatial and temporal patterning. *Semin. Cell Dev. Biol.* **142**, 54–66 (2023).
20. Holguera, I. & Desplan, C. Neuronal specification in space and time. *Science* **362**, 176–180 (2018).
21. Chen, Y.-C. & Desplan, C. Gene regulatory networks during the development of the Drosophila visual system. *Curr. Top. Dev. Biol.* **139**, 89–125 (2020).
22. Fernandes, V. M., Chen, Z., Rossi, A. M., Zipfel, J. & Desplan, C. Glia relay differentiation cues to coordinate neuronal development in Drosophila. *Science* **357**, 886–891 (2017).

23. Chen, Z. *et al.* A Unique Class of Neural Progenitors in the Drosophila Optic Lobe Generates Both Migrating Neurons and Glia. *Cell Rep.* **15**, 774–786 (2016).

24. Bertet, C. *et al.* Temporal Patterning of Neuroblasts Controls Notch-Mediated Cell Survival through Regulation of Hid or Reaper. *Cell* **158**, 1173–1186 (2014).

25. Pinto-Teixeira, F. *et al.* Development of Concurrent Retinotopic Maps in the Fly Motion Detection Circuit. *Cell* **173**, 485-498.e11 (2018).

26. Apitz, H. & Salecker, I. A region-specific neurogenesis mode requires migratory progenitors in the Drosophila visual system. *Nat. Neurosci.* **18**, 46–55 (2015).

27. Apitz, H. & Salecker, I. Spatio-temporal relays control layer identity of direction-selective neuron subtypes in Drosophila. *Nat. Commun.* **9**, 2295 (2018).

28. Valentino, P. & Erclik, T. Spalt and disco define the dorsal-ventral neuroepithelial compartments of the developing Drosophila medulla. *Genetics* **222**, iyac145 (2022).

29. Erclik, T. *et al.* Integration of temporal and spatial patterning generates neural diversity. *Nature* **541**, 365–370 (2017).

30. Li, X. *et al.* Temporal patterning of Drosophila medulla neuroblasts controls neural fates. *Nature* **498**, 456–462 (2013).

31. Suzuki, T., Kaido, M., Takayama, R. & Sato, M. A temporal mechanism that produces neuronal diversity in the Drosophila visual center. *Dev. Biol.* **380**, 12–24 (2013).

32. Konstantinides, N. *et al.* A complete temporal transcription factor series in the fly visual system. *Nature* **604**, 316–322 (2022).

33. Zhu, H., Zhao, S. D., Ray, A., Zhang, Y. & Li, X. A comprehensive temporal patterning gene network in Drosophila medulla neuroblasts revealed by single-cell RNA sequencing. *Nat. Commun.* **13**, 1247 (2022).

34. Chang, T., Mazotta, J., Dumstrei, K., Dumitrescu, A. & Hartenstein, V. Dpp and Hh signaling in the Drosophila embryonic eye field. *Development* **128**, 4691–4704 (2001).

35. Hasegawa, E. *et al.* Concentric zones, cell migration and neuronal circuits in the Drosophila visual center. *Development* **138**, 983–993 (2011).

36. M, C. & C, D. Coordination between stochastic and deterministic specification in the Drosophila visual system. *Science* **366**, (2019).

37. Naidu, V. G. *et al.* Temporal progression of Drosophila medulla neuroblasts generates the transcription factor combination to control T1 neuron morphogenesis. *Dev. Biol.* **464**, 35–44 (2020).

38. Chyb, S. & Gompel, N. Wild-type morphology. in *Atlas of Drosophila Morphology* (eds. Chyb, S. & Gompel, N.) 1–23 (Academic Press, San Diego, 2013). doi:10.1016/B978-0-12-384688-4.00001-8.

39. Gunawan, F., Arandjelovic, M. & Godt, D. The Maf factor Traffic jam both enables and inhibits collective cell migration in Drosophila oogenesis. *Dev. Camb. Engl.* **140**, 2808–2817 (2013).